75th International Astronautical Congress (IAC), Milan, Italy, 14-18 October 2024.

IAC-24-C4.5

Gasdynamic expansion models and preliminary heat transfer and thermal analysis for the nozzle of a Microwave Electrothermal Thruster using different propellants

Michele Nava[a]*, Filippo Maggi[a], Davide Zuin[b]

[a] *Department of Aerospace Science & Technology, Politecnico di Milano, Via La Masa 34, 20156 Milano*
[b] *D-Orbit S.p.A., Viale Risorgimento, 57, 22073 Fino Mornasco CO*

* Corresponding Author, michele1.nava@polimi.it

Abstract

The Microwave Electrothermal Thruster (MET) is an emerging technology for space propulsion that uses microwave power to heat a gas inside a cylindrical resonant cavity, before accelerating it through a converging-diverging nozzle to supersonic velocities, producing thrust. The nature of the gasdynamic expansion is crucial in determining the nozzle exit conditions and the propulsive performances of the thruster. Chemical reactions in MET nozzles may be favored by the high nozzle-inlet temperatures generated in the resonant cavity, but the high gas velocities and the small size of the nozzles themselves reduce the time available for chemical reactions to occur. Moreover, heat transfer to the nozzle walls and temperature limits of nozzle materials can impose severe constraints on the working conditions and maximum achievable thruster performance.

Different models are applied and compared to describe the gasdynamic expansion of N_2, N_2O and H_2O for various nozzle inlet conditions: a frozen chemistry model, a chemical equilibrium model, and a hybrid model employing the Bray freezing criterion to identify a transition point from chemical equilibrium to frozen flow conditions. The latter is validated using the quasi-1D inviscid Euler equations with chemical reactions for the case of N_2. Convective heat transfer from the expanding gas to a radiatively cooled nozzle is modelled and simulated for the Bray expansion of H_2O, considering a stagnation temperature and pressure of 6000 K and 1 atm, respectively.

The Bray model predicts a freezing point close to the nozzle throat and shifted towards the converging section for all the propellants and most chamber conditions, indicating an almost entirely frozen expansion. The heat transfer model predicts large power losses to the nozzle walls, suggesting the need to include them in the gasdynamic expansion modeling and to investigate regenerative nozzle cooling systems for future high performance METs.

Keywords: Microwave Electrothermal Thruster, nozzle expansion, Bray, electric propulsion, heat transfer

1. Introduction

Within the last decade, an increased interest to bridge the gap between electric propulsive (EP) subsystems, which can provide high specific impulse values and low thrusts, and chemical propulsive (CP) subsystems, which provide the opposite, has been registered. CP technologies for satellite applications have been demonstrated to deliver theoretical performances in vacuum which exceed specific impulses of 300 s and thrust values in the order of hundreds of newtons for short timespans (minutes) [1]. This enables satellites to perform rapid maneuvers in space, when needed, with limited impact on the overall satellite power budget. On the other hand, EP engines can achieve much higher specific impulses (>1000 s), thanks to the propellant and power source decoupling. However, significant power demands are needed, in the order of kW, to achieve thrust values in the range of tens of mN [2]. Moreover, traditional EP technologies have often also been hindered by the presence of performance- and/or life-limiting elements, such as heaters, electrodes, grids, etc., and by their architectural complexity [3].

Among the new EP technologies which are being developed and are theoretically capable of covering this performance gap, the MET represents an interesting choice because of its design simplicity (also due to the use of a traditional solid nozzle to accelerate the propellant), the ability to work at different frequencies and on multiple propellants [4, 5], and most importantly, no theoretical performance limitation thanks to the absence of electrodes and heating elements [5].

The MET (Fig.1) is composed by a cylindrical resonant cavity made of a conductive material, closed by two circular endplates, and divided in half by another plate made of dielectric material. An antenna is placed on the central axis at one cavity end and introduces microwave power in the cavity. The propellant is introduced with a tangential velocity in the other cavity half, where a plasma is ignited and sustained by the electromagnetic field generated by the antenna [5]. The propellant swirls around the plasma and is heated to high temperatures, right before reaching the nozzle inlet, located on the cavity axis at the endplate opposite to the

antenna. The propellant is then accelerated and expelled at high velocities through the nozzle, producing thrust.

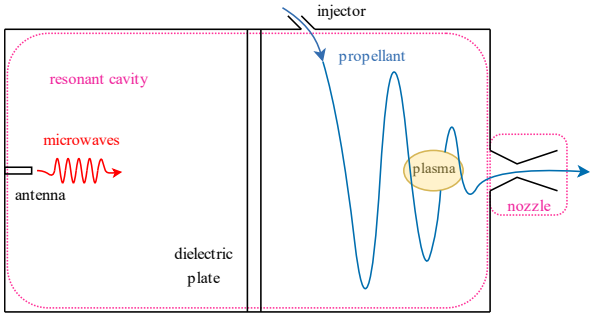

Figure 1 – MET scheme

Preliminary results from literature studies show that the technology is theoretically capable of achieving specific impulses larger than 800 s and thrust in the order of hundreds of millinewtons [4, 5, 6]. Furthermore, the implementation of propellants which are already used by CP subsystems, could ease the integration of MET units on existing propulsive systems, with minimal impacts at system level. The potential integration of METs with specific impulse of 600-700 s or larger on existing satellites becomes interesting when considering the new-space market, which is significantly driven by the need of rapid service delivery and cost reductions. The MET technology could allow satellite companies to significantly improve the time-to-market due to the increased thruster performances, both in terms of specific impulse and thrust, and lower the cost of satellite manufacturing, as the overall mass and volume to perform a specific mission would be reduced.

Among the several propellants that have been proposed for MET, we focus here on water vapour (H_2O), nitrous oxide (N_2O) and nitrogen (N_2). Examples of METs with specific impulse above 800 s have been reported in the literature using H_2O [6] which is a candidate to be the ideal MET propellant, not only for the expected high performance, but also for its low cost, high density at ambient conditions and consequent ease of storage, non-toxicity, and abundance in the solar system, which could enable the possibility of in-situ resource utilization (ISRU). On the other hand, N_2O is a non-toxic fluid with interesting properties in terms of self-pressurization: it is increasingly being implemented in new CP units as an oxidizer alternative to harmful substances in both monopropellant and bipropellant applications [7]. Furthermore, N_2O has already been tested and studied in METs, as reported by literature sources [4]. The possibility of implementing nitrous oxide among different technologies on a same satellite platform is pivotal for space missions and applications, as it allows to expand the multi-mode framework associated to nitrous-based propulsive subsystems. Beneficial effects of multimode propulsive systems on orbit raising, cislunar and interplanetary missions are already present in literature reviews [8]. Finally, nitrogen has mostly been used to develop and test the models presented in this work, because it is much simpler to treat than water and nitrous oxide yet shares with them the common features of a molecular gas, i.e., the possibility to undergo dissociation and recombination processes.

Most theoretical studies on MET have focused on modeling and simulation of the resonant cavity, often using very simple descriptions of the nozzle expansion. Some recent, remarkable efforts have been carried out to study the coupled system of fluid dynamics and plasma behavior in the entire MET domain, providing insight on the flow properties both in the resonant cavity and in the nozzle [9,10]. So far, these works have been limited to monoatomic gases, because of their simplicity and reduced number of reactions (i.e., ionization and excitation processes). However, the analysis of the gas dynamic expansion in the nozzle is crucial and needed also for molecular gases to determine the flow exit conditions and the propulsive performance of METs. Furthermore, based on previous studies [4], we can expect that the flow temperatures required to obtain high specific impulses can reach thousands of K. Combined with the reduced size of MET nozzles, necessary to obtain very small flowrates typical of MET operation [4], we must also consider that some performance limitations may arise due to nozzle material constraints and heat dissipation through the nozzle walls. In this work we develop models and tools to describe the nozzle expansion and the fluid-wall thermal interaction using water, nitrogen, and nitrous oxide, with the goal to provide some insight on the behavior of these propellants and identify potential performance limitations due to thermal constraints. The same procedures can be applied in general to any propellant in MET nozzles and other micronozzles for high-enthalpy flows.

2. Material and methods

2.1 Figures of merit

There are different parameters which can be used to assess the performance of space propulsion units [11]: in this work we mostly use the specific impulse, which we can define after having introduced the definition of thrust.

The thrust (τ) is the additional force experienced by the spacecraft when the propellant is accelerated and

ejected through the nozzle and is composed of a static component and a momentum component. The former is going to be neglected in this work because the considered pressure at the nozzle outlet is very low. Thrust is thereby computed as:

$$\tau = \dot{m} v_{ex} \qquad (1)$$

where $\dot{m}$ is the propellant mass flow rate and v_{ex} is the propellant velocity at the nozzle outlet. The thrust is measured in Newtons.

The specific impulse (I_{sp}), is defined as the ratio between the thrust and the weight of propellant mass flow rate evaluated on the Earth at sea level. Again, neglecting the thrust static contribution, the specific impulse is obtained as:

$$I_{sp} = \frac{\tau}{\dot{m} g_0} = \frac{v_{ex}}{g_0} \qquad (2)$$

where g_0 is the standard acceleration due to gravity on Earth at sea level. The I_{sp} is measured in seconds.

The specific power or specific energy ($P_{in}/\dot{m}$) is defined as the ratio between the input electromagnetic power (P_{in}) transferred to the propellant and the propellant mass flow rate, and is a useful quantity often found in studies on the MET.

2.2 Methods

In this work, the MET has been analysed by decoupling the resonant chamber and the nozzle. The resonant cavity modelling has first been used to determine the conditions at the nozzle inlet and the specific power required to obtain those conditions. The propellant expansion in the nozzle has then been studied with different models and, finally, a preliminary study on heat transfer and thermal analysis in the nozzle walls has been conducted.

2.2.1 Resonant cavity modelling

The resonant cavity has been treated as a simple heat exchanger, where the microwave power is transferred to the propellant and heats it from a *reference state* to the *chamber conditions*, changing not only the temperature and pressure, but also the composition. As in other studies on MET [12], it is assumed that the residence time of the propellant inside the resonant cavity is much higher than the time required by the propellant mixture to reach chemical equilibrium. Thus, for a given propellant and a certain value of chamber temperature T_c and pressure p_c, the composition and mixture properties are determined by applying the laws of chemical equilibrium (see section 3.1). This thermodynamic state also provides the nozzle inlet conditions. A simple power balance equation is used to determine the specific power required to heat the propellant from the reference conditions to the chamber conditions:

$$\frac{P_{in}}{\dot{m}} = h_c - h_{ref} \qquad (3)$$

where h_c and h_{ref} are the specific enthalpy per unit mass of reactants at the chamber and reference conditions, respectively, with respect to the standard state (i.e., $T = 298.15\ K$ and $p = 1\ atm$). Equation (3) assumes that all the microwave input energy is transferred to the propellant in the form of heat and is used solely to raise its enthalpy, with negligible velocity variation between the resonant cavity inlet and outlet and no power loss to the cavity walls. Table 1 summarizes the reference conditions used for the propellants of interest and the corresponding specific enthalpy: note that these correspond to the standard state for N_2 and N_2O [13] and to a given condition computed using the chemical equilibrium model (see section 3.1) for H_2O at higher temperature, so to reproduce the fact that water should already be in the gaseous state when entering the resonant cavity.

Table 1. Reference conditions for the used propellants

	$p_{ref}\ [atm]$	$T_{ref}\ [K]$	$h_{ref}[kJ/kg]$
N_2	1	298.15	0
N_2O	1	298.15	1876.5
H_2O	1	398.15	-13235.3

2.2.2 Nozzle expansion analysis

We have developed and applied different quasi-one-dimensional, axisymmetric models (described in detail in section 3.2), to study the nozzle expansion. All models assume that the propellant can be described as an ideal gas or as a mixture of ideal gases. The first two models share the hypothesis of isentropic expansion: one considers a frozen chemical composition throughout the entire expansion (*frozen* model), while the other assumes that chemical reactions are fast enough to maintain chemical equilibrium in every point of the expansion (*shifting equilibrium* model). A third, hybrid-model is then developed, in which the expansion is treated as the one in chemical equilibrium in the first section of the nozzle, and as the frozen one in the second section: the transition point from one regime to the other is determined using a Bray sudden freezing criterion [14]

(*Bray* model). Finally, a more precise model using the inviscid Euler equations with chemical reactions has been developed for the case of N_2 only (*Euler* model).

The Bray model has initially been validated by applying it to a representative case of a N_2 expansion and comparing its solution to the more precise one obtained using the *Euler* model. It has then been applied to N_2, N_2O and H_2O for a wide range of nozzle inlet conditions, to estimate the specific impulse as a function of the chamber conditions and evaluate if the expansion is closer to the frozen or the shifting equilibrium one.

The nozzle used for the simulations on all propellants is a converging-diverging conical nozzle, with a cone half-angle $\theta = 15°$ and a nozzle throat diameter $D^* = 1\ mm$, a dimension comparable to that of other MET nozzles [4]. The nozzle expansion ratio, defined as the ratio between the cross section at a given point (A) and that at the throat ($A^* = \pi {D^*}^2/4$) can be related to the axial coordinate x through:

$$\frac{A}{A^*} = 1 + 4\left(\frac{\theta x}{D^*}\right)^2 \quad (4)$$

where $x = 0$ corresponds to the throat section. The x coordinate corresponding to a given expansion ratio is obtained by inverting relation (4) and taking the negative or positive value of x if the point is in the converging or diverging section of the nozzle, respectively. The nozzle diameter at each point (D) is simply $D = \sqrt{4\pi A}$.

In all simulations the chamber pressure has been set to 1 atm, which is a typical value for MET operation [4,5], and the exit pressure to 1 Pa, which to a first approximation represents an expansion towards vacuum but is high enough to guarantee that the models work, and the continuum hypothesis remains verified.

2.2.3 Thermal analysis

A heat transfer model (section 3.3) has been developed and applied to perform a preliminary, steady-state thermal analysis of the solid nozzle walls in the case of a radiatively cooled nozzle. The goal of this analysis is to determine the convective heat flux delivered from the gas to the nozzle walls and estimate the inner and outer nozzle wall temperatures along the entire nozzle axis. Two tungsten nozzles with constant wall thicknesses of 1 mm and 5 mm have been used for the simulations. Tungsten has been selected as it is a material that can withstand extreme temperatures and is a candidate to be used in future MET nozzles. Among the previously studied expansions, the one using the shifting equilibrium model with H_2O, and a chamber temperature $T_c = 6000\ K$ has been selected as a representative case study.

3. Theory and calculation

3.1 Chemical equilibrium in the resonant cavity

As mentioned previously, we assume that the propellant residence time in the MET resonant cavity is much higher than that required for chemical reactions to occur. This condition is referred to as *chemical equilibrium* [15]. To fully characterize the propellant state at the chamber conditions (i.e., assigned p_c and T_c), we must solve the composition problem, which means determining the molar fraction of each product species at those given thermodynamic conditions. For a mixture with NS possible product species, we can define the molar fraction X_j of each component j as the ratio between the number of moles n_j of that component and the total number of moles n:

$$X_j = \frac{n_j}{n} = \frac{n_j}{\sum_{i=1}^{NS} n_i} \quad (5)$$

Methods based on free-energy-minimization allow to solve the composition problem without the need to define a set of possible chemical reactions a priori. In this work, we employ the *assigned temperature and pressure* package of the CEA code by Gordon & McBride [16], which uses the minimization of Gibbs-free-energy, to determine the mixture composition, including ions as possible reaction products.

Among other relevant thermodynamic quantities, the CEA code also provides the specific enthalpy per unit mass of reactants (h_c) with respect to the standard state, computed as a molar-averaged quantity [16], which can be used with equation (3) to obtain the specific power.

3.2 Gas dynamic nozzle expansion models

3.2.1 Frozen model

It is the simplest and most used model to provide a first approximation of nozzle flows. This model assumes that the expansion is isentropic, and the chemical composition remains fixed and equal to that at the nozzle inlet (i.e., the time required for chemical reactions to occur is much larger than the flow characteristic time [15]). Assuming a null initial velocity ($v_c = 0$), it can be shown [11] that the velocity v at a point with given pressure p is:

$$v = \sqrt{\frac{2\gamma}{\gamma - 1}\frac{\Re T_c}{\mathcal{M}}\left[1 - \left(\frac{p}{p_c}\right)^{(\gamma-1)/\gamma}\right]} \quad (6)$$

where $\Re$ is the universal gas constant (for calculations in this work $\Re = 8.3145\, J\, mol^{-1}K^{-1}$), and γ and $\mathcal{M}$ are the mixture specific heat ratio and molar mass, respectively. The latter are also assumed to remain constant throughout the expansion and are computed through a molar weighted average of the individual species quantities γ_j and $\mathcal{M}_j$, namely:

$$\gamma = \sum_{j=1}^{NS} X_j \gamma_j \qquad (7)$$

$$\mathcal{M} = \sum_{j=1}^{NS} X_j \mathcal{M}_j \qquad (8)$$

The values of specific heat ratio and molar mass for the individual species used in this work are shown in Table 2.

Table 2. Specific heat ratio and molar mass for the individual species of interest

Species	$\gamma\ [-]$	$\mathcal{M}\ [g/mol]$
N, N^+	5/3	14
N_2, N_2^+	7/5	28
N_2O	1.31	44
NO, NO^+	7/5	30
O, O^+	5/3	16
O_2	7/5	32
OH	1.384	17
H, H^+	5/3	1
H_2	7/5	2
HO_2	1.31	33
H_2O_2	1.267	34
H_2O	1.31	18

The nozzle exit velocity can be obtained using equation (6) with pressure equal to the exit pressure p_{ex}.

3.2.2 Shifting equilibrium model

This model shares the isentropic hypothesis with the previous one, but it assumes that the characteristic time of chemical reactions throughout the expansion is much lower than that of the flow [15], and thereby chemical equilibrium is maintained at every location along the nozzle. The composition changes during the expansion and the decreasing temperature generally favours recombination processes, which allow to recover sensible enthalpy, contributing to higher temperatures and exit velocities than those predicted by the frozen model. The shifting equilibrium model is implemented using the *assigned entropy and pressure* package of the CEA code, which can compute the chemical equilibrium composition and thermodynamic state of a mixture at a given pressure and entropy [16]. The propellant conditions are retrieved on a grid of points with progressively decreasing pressure from 1 atm to 1 Pa, and fixed entropy equal to that at the nozzle inlet. The velocity v at all points on this grid is computed using the conservation of the total enthalpy and assuming a null velocity at the nozzle inlet:

$$v = \sqrt{2(h_c - h)} \qquad (9)$$

where h is the specific enthalpy obtained at a given pressure p. The nozzle exit velocity can be found using equation (9) with the value of specific enthalpy h_{ex} found for the exit pressure p_{ex}. To link every point on the grid to the corresponding area expansion ratio A/A^*, the following procedure is applied. First, the sound velocity (a) at all points is retrieved from the CEA code and the Mach number is computed as:

$$Mach = \frac{v}{a} \qquad (10)$$

The grid is then refined where the Mach number is closer to unity until the last subsonic point ($Mach < 1$) and the first supersonic point ($Mach > 1$) have a sufficiently small pressure difference ($|\Delta p| = 100\ Pa$): a linear interpolation between the properties of these two points is then performed to obtain the throat conditions (corresponding to $Mach = 1$). Finally, the expansion ratio is obtained using a rearrangement of the mass conservation equation ($\dot{m} = \rho v A = const$):

$$\frac{A}{A^*} = \frac{\rho^* v^*}{\rho v} \qquad (11)$$

where ρ is the density at the considered point, and ρ^* and v^* are the density and velocity at the throat, respectively.

3.2.3 Bray model

It is known [15] that the frozen model and the shifting equilibrium model represent the lower and upper performance limits of the isentropic theory, and that the exact, non-isentropic solution with a finite chemistry rate must lie somewhere in between them. It was first hypothesized by Bray [14] that we can assume the flow to be in chemical equilibrium in the first part of the nozzle, where the velocity is low, and chemically frozen in the second part, where the velocity is much higher. We can identify a *sudden freezing point*, where the flow transitions instantly from the first kind to the second. This procedure does not allow to precisely represent the flow behavior in the transition region, but can more accurately

predict the nozzle exit conditions, as it keeps into account that at least a part of the reaction enthalpy is recovered in the initial phase of the expansion. The expansion with this model is obtained by first repeating the steps of the previous section and obtaining the shifting equilibrium flow; a freezing point (*FP*) is then identified somewhere along the shifting equilibrium expansion using a *freezing criterion*; the remaining part of the expansion after the freezing point is obtained using the frozen flow assumption and the isentropic relations [11] referring to the FP as the starting point. Note that the velocity at points in the frozen section (including the exit velocity) can therefore be computed as a function of the pressure p:

$$v = \sqrt{\frac{2\gamma_{FP}}{\gamma_{FP}-1}\frac{\Re T_{FP}}{\mathcal{M}_{FP}}\left[1-\left(\frac{p}{p_{FP}}\right)^{\frac{\gamma_{FP}-1}{\gamma_{FP}}}\right]+v_{FP}^2} \quad (12)$$

where quantities with the subscript *FP* are evaluated at the freezing point.

The freezing criterion generally requires identifying one or more dominant chemical reactions (either from an energetic point of view or based on relative abundance of the present species) and find where the rate of such reactions becomes lower than the rate required to maintain chemical equilibrium [15]. The dominant reactions are typically the recombination reactions of the kind: $A + B + M \rightleftharpoons C + M$, where two species ($A$ and B) react with a third body (M) to produce the recombined species (C). Denoting by $k_{f,M}$ and $k_{b,M}$ the forward and backward reaction coefficients with a specific third body M, respectively, it is known that for a mixture in chemical equilibrium the following relation holds:

$$k_{f,M}[A]_{eq}[B]_{eq}[M]_{eq} = k_{b,M}[C]_{eq}[M]_{eq} \quad (13)$$

where $[...]_{eq}$ indicates the instantaneous molar concentration value of a certain species under the condition of chemical equilibrium [15]. For a generic species J:

$$[J]_{eq} = \left\{\frac{\rho}{\mathcal{M}}X_J\right\}_{eq} \quad (14)$$

where again, the expression $\{...\}_{eq}$ indicates that all quantities within brackets are evaluated in chemical equilibrium conditions (i.e., with the shifting equilibrium model in our case). In this work we have considered three reactions for the different propellants (each of which can happen with a certain set of third bodies, visible in Table 3):

- recombination of H and OH radicals into H_2O
- recombination of atomic nitrogen into N_2
- recombination of atomic oxygen into O_2

The first and the second have been used for H_2O and N_2 propellants, respectively. For N_2O propellant, based on relative abundance of the reacting species, the second and the third reactions have been used at high temperature ($T_c \geq 7000\,K$) and low temperature ($T_c < 7000K$), respectively. The freezing criterion has been applied by taking as the FP the first point in the flow to satisfy the condition:

$$\sum_{M\in TB} k_{b,M}[C]_{eq}[M]_{eq} \leq \left\{\rho v\frac{\partial(X_C/\mathcal{M})}{\partial x}\right\}_{eq} \quad (15)$$

where TB denotes the set of all third bodies considered for a certain reaction. The backward rate coefficients used in this work have the Arrhenius form:

$$k_{b,M} = C_{b,M}T^{\eta_k}\exp\left(-\frac{\theta_k}{T}\right) \quad (16)$$

for which the values of the coefficients $C_{b,M}$, η_k and θ_k can be found in Table 3. The differential term $\partial(X_C/\mathcal{M})/\partial x$ has been approximated using a centred finite-difference scheme, and it has been verified for all studied cases that the pressure difference between that at

Table 3. Reactions and corresponding coefficients [17,18]

Reaction	Third body M	$C_{b,M}$ $[m^3mol^{-1}s^{-1}]$	η_k $[-]$	$\theta_k[K]$
$N+N+M \rightleftharpoons N_2+M$	N_2, O_2, NO	7×10^{15}	-1.6	113200
	N, O	3×10^{16}	-1.6	113200
$O+O+M \rightleftharpoons O_2+M$	N_2, O_2, NO	2×10^{21}	-1.5	59500
	N, O	1×10^{16}	-1.5	59500
$H+OH+M \rightleftharpoons H_2O+M$	$H, HO_2, H_2, H_2O, H_2O_2, O, OH, O_2, H^+, O^+$	2×10^{16}	-1.5	57417

the FP and that at both the point preceding it and the one following it is $|\Delta p| < 1000\ Pa$.

3.2.4 Euler model

This model starts from the steady-state form of the quasi-1D Euler equations with chemical reactions [19]:

$$\begin{cases} \frac{d(\rho v A)}{dx} = 0 \\ \rho v \frac{dv}{dx} = -\frac{dp}{dx} \\ \rho v \frac{de}{dx} = -p\frac{dv}{dx} - pv\frac{d(lnA)}{dx} \\ \frac{d(\rho_i v A)}{dx} = \dot{\omega}_i A \end{cases} \quad (17)$$

where e is the internal energy, ρ_i is the partial density of species i ($\rho_i = \rho Y_i$, with Y_i mass fraction of species i) and $\dot{\omega}_\iota$ is the production rate of species i (which can be determined once the set of reactions involving that species is chosen and the corresponding reaction rates are known [15]). In this work we consider the simple case of an ideal nitrogen gas which can undergo dissociation and recombination; thus, the present species are N and N_2. We denote by Y the mass fraction of N (the mass fraction of N_2 is simply $1 - Y$) and model the internal energy as:

$$e = Y\left(\frac{3}{2}R_N T + \frac{\Delta_f H_N^0}{\mathcal{M}_N}\right) + \frac{5}{2}R_{N_2}T(1-Y) \quad (18)$$

where $R_j = \Re/\mathcal{M}_j$ is the specific gas constant for species j (note that $R_N = 2R_{N_2}$) and $\Delta_f H_N^0 = 472.445\ kJ/mol$ is the standard enthalpy of formation of N [13]. Note that the mass fraction Y can be related to the molar fraction of atomic nitrogen through $Y = X_N\mathcal{M}_N/\mathcal{M}$. We only consider the reactions of the kind $2N + M \rightleftharpoons N_2 + M$ with third bodies $M = N, N_2$. It can then be shown that the production rate of atomic nitrogen is:

$$\dot{\omega}_N = 2\mathcal{M}_N\left(k_{b,N_2}[N_2] + k_{b,N}[N]\right)([N_2] - K_c[N]^2) \quad (19)$$

where again $k_{b,M}$ is the backward rate coefficient for the reaction happening with the third body M, the expression [...] now denotes the instantaneous mass concentration ($[J] = \rho Y_J/\mathcal{M}_J$), and K_c is the *equilibrium constant* of the recombination reaction ($K_c = k_{f,M}/k_{b,M}$). The backward rate coefficients $k_{b,M}$ are computed as in equation (16) and with the coefficients $C_{b,M}$, η_k and θ_k from Table 3. We use a Lighthill model [20] for the equilibrium constant, which is only function of the temperature:

$$K_c(T) = \frac{2\rho_D}{\mathcal{M}_N}\exp\left(\frac{\theta_k}{T}\right) \quad (20)$$

where $\rho_D = 1.3 \times 10^5\ kg/m^3$.

Under these assumptions, the system of equations (17) can be conveniently recast as a system of ordinary differential equations (ODE) in the variables Y, v, ρ, T (see Appendix A).

The Euler model has only been applied to the case of an expansion starting from equilibrium chamber conditions of $T_c = 8000\ K$ and $p_c = 1\ atm$, and the system of equations has been solved using MATLAB and the ode23s solver. Direct integration from the chamber conditions is not possible because setting the initial velocity to zero would create singularities in the ODE system. Therefore, the initial conditions were obtained using the first point at non-zero velocity computed using the shifting equilibrium model, at a pressure $p_0 = 101320\ Pa$. The corresponding initial values of the state vector are $Y_0 = 0.82229$, $v_0 = 40\ m/s$, $\rho_0 = 2.3338 \times 10^{-2}\ kg/m^3$, and $T_0 = 7999.98\ K$.

3.3 Heat transfer model

This model considers only heat transfer in the radial direction and more specifically a convective heat transfer between the fluid and the nozzle walls, a conductive heat transfer within the nozzle solid material, and a radiative heat transfer from the outer nozzle walls towards deep space. Each section of the nozzle is treated as a hollow cylinder, and the heat rate per unit length transferred through the nozzle walls ($\dot{q}'$) is computed as:

$$\dot{q}' = \frac{T_{gas} - T_{w,in}}{\frac{1}{2\pi R_{in} h_g}} = \frac{T_{w,in} - T_{w,out}}{\frac{\ln(R_{out}/R_{in})}{2\pi\lambda_w}} = \frac{\varepsilon_w \sigma T_{w,out}^4}{\frac{1}{2\pi R_{out}}} \quad (21)$$

where T_{gas} is the gas temperature on the nozzle axis, $T_{w,in}$ and $T_{w.out}$ indicate the temperature on the inner and outer surfaces of the nozzle, respectively, $R_{in} = D/2$ and $R_{out} = R_{in} + t_w$ are the inner and outer nozzle radii, respectively, and t_w is the nozzle thickness. The quantities $\lambda_w = 175\ Wm^{-1}K^{-1}$ and $\varepsilon_w = 0.45$ are the values assumed for the nozzle thermal conductivity and emissivity, respectively, and $\sigma \approx 5.67 \times 10^{-8}\ Wm^{-2}K^{-4}$ is the Stefan-Boltzmann constant. The term h_g is the convective heat transfer coefficient, which has been modelled using the Sieder-Tate laminar correlation [21]:

$$h_g = \frac{\lambda}{D}1.86\left(RePr\frac{D}{L}\right)^{\frac{1}{3}}\left(\frac{\mu}{\mu_w}\right)^{0.14} \quad (22)$$

where λ is the thermal conductivity of the propellant, $Re = \rho v D/\mu$ and $Pr = c_p \mu/\lambda$ are the Reynolds and Prandtl numbers (c_p is the specific heat at constant pressure), respectively, L is the distance from the nozzle inlet, and μ and μ_w are the gas viscosity at the nozzle axis and at the inner wall surface. A laminar heat transfer correlation has been selected after having checked that for the selected case study the Reynolds number throughout the entire expansion remains low enough to guarantee that the flow is laminar. The properties λ, μ, and c_p of the mixture are obtained directly from the CEA code in the shifting equilibrium section of the expansion using the values *with equilibrium reactions* provided by the code [16]. In the frozen section, they are again computed as explained in [16], i.e., through a molar average and using a mixing rule on the same quantities obtained for the individual species ($C_{p,i}^{\circ}$, μ_i, λ_i), but only considering the *frozen* term contribution for specific heat and thermal conductivity [16]:

$$\begin{cases} c_p = \frac{\sum_{i=1}^{NS} X_i C_{p,i}^{\circ}}{\mathcal{M}} \\ \mu = \sum_{i=1}^{NS} \frac{X_i \mu_i}{X_i + \sum_{j=1, j\neq i}^{NS} X_j \phi_{ij}} \\ \lambda = \sum_{i=1}^{NS} \frac{X_i \lambda_i}{X_i + \sum_{j=1, j\neq i}^{NS} X_j \psi_{ij}} \end{cases} \qquad (23)$$

where the expressions for $C_{p,i}^{\circ}$, μ_i, λ_i, ϕ_{ij} and ψ_{ij} can be found in [16] and the corresponding coefficients in [22, 23]. The viscosity at the inner wall along the entire expansion is computed in the same way as the viscosity on the nozzle axis in equation (23) but using the temperature $T_{w,in}$ in place of T_{gas} in the corresponding correlations of the $\mu_i$for the individual species. Equation (21) has been rewritten as a system of two non-linear algebraic equations in the unknowns $T_{w,in}$ and $T_{w,out}$, and has been solved using the *fzero* solver in MATLAB. Finally, the total power dissipated through the nozzle (P_{diss}) can be obtained by integrating the heat rate per unit length on the nozzle length:

$$P_{diss} = \int_0^{L_{nozzle}} \dot{q}' dx \qquad (24)$$

where L_{nozzle} is the total nozzle length, while the heat flux across the inner nozzle surface is computed as:

$$\dot{q}''_{w,in} = \dot{q}'/(2\pi R_{in}) \qquad (25)$$

4. Results and Discussion

4.1 Chamber chemical composition

The chemical composition of N_2, N_2O and H_2O is shown as a function of chamber temperature in Fig. 2-4, for temperatures ranging from 500 K to 10000 K. It can be seen for all propellants that, as temperature increases, the composition shifts towards a more and more dissociated one, favouring the presence of atomic species over molecules. A very small number of ions begins to be present for all propellants above 9000 K.

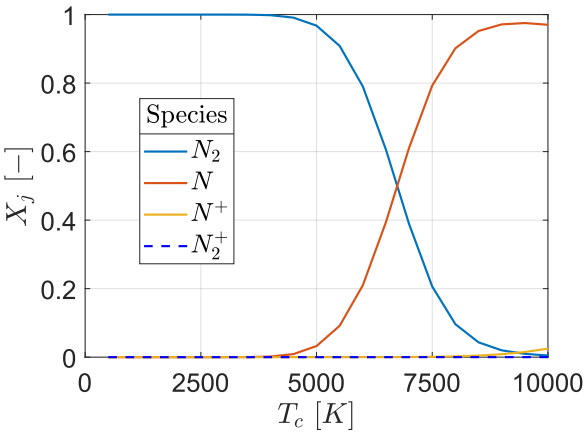

Figure 2 – Molar composition as a function of chamber temperature (N_2 propellant, $p_c = 1\ atm$)

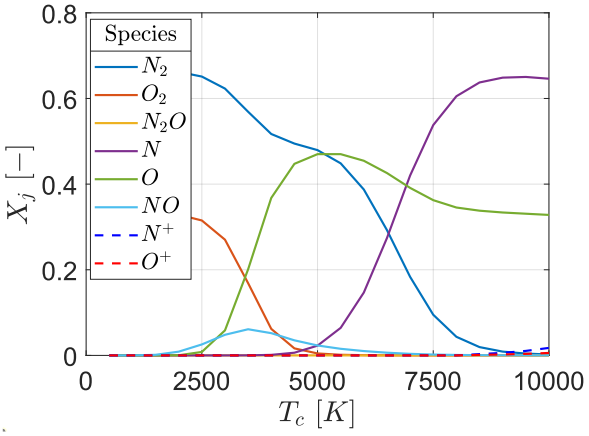

Figure 3 – Molar composition as a function of chamber temperature (N_2O propellant, $p_c = 1\ atm$)

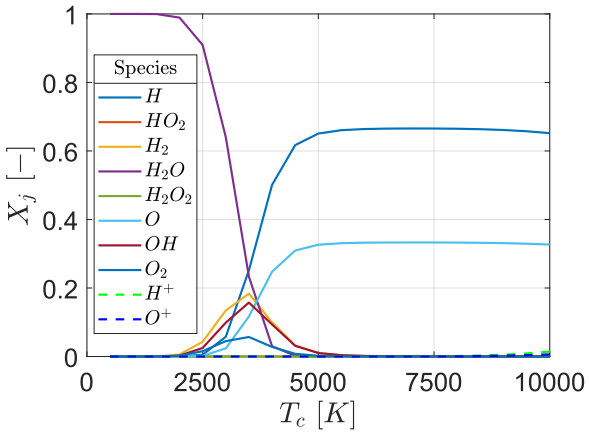

Figure 4 – molar composition as a function of chamber temperature (H_2O propellant, $p_c = 1\ atm$)

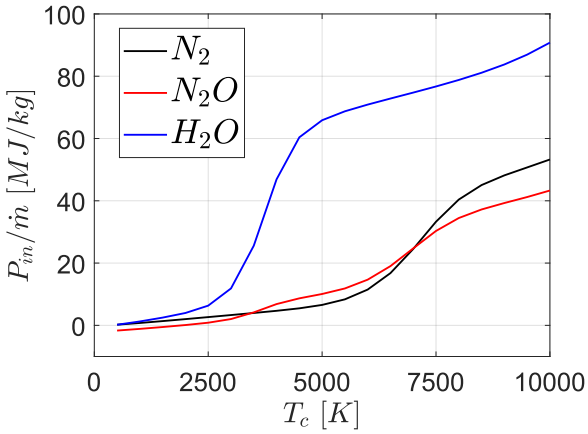

Figure 5 – Specific power as a function of chamber temperature for different propellants ($p_c = 1\ atm$)

The specific power required to bring the propellant to the desired chamber temperatures, computed by means of equation (3), is shown for the three propellants in Fig. 5. N_2 and N_2O require a similar amount of specific power for a given T_c. On the other hand, H_2O requires much more specific power to obtain the same chamber temperature. Note that the curve for N_2O starts from negative values of specific power: this is due to the fact that the predicted equilibrium composition has a null concentration of N_2O even at low temperatures, and thus all the formation enthalpy stored in the N_2O molecule (about $2\ MJ/kg$) is released in its exothermic dissociation ($N_2O \rightarrow N_2 + \frac{1}{2}O_2$). In Fig. 5, regions with different slope are present for each propellant: the steeper regions correspond to those temperature intervals where a big part of the input power is being used for an important dissociation reaction: the dissociation of O_2 ($2500\ K < T_c < 5000\ K$, N_2O propellant), the dissociation of N_2 ($5000\ K < T_c < 9000\ K$, N_2 and N_2O propellants), and the dissociation of H_2O ($2000\ K < T_c < 5000\ K$, H_2O propellant).

4.2 Validation of the Bray model

As mentioned previously, the expansion of a N_2 propellant from chamber conditions of $T_c = 8000\ K$ and $p_c = 1\ atm$, has been used to validate the Bray model against the Euler model, and compare the results to the limit solutions provided by the frozen and the shifting equilibrium model. The application of the freezing criterion (equation (15)) to identify the freezing point is shown in Fig. 6. The third body which mostly contributes to the recombination reactions is atomic nitrogen, and the freezing point is estimated to be very close to the throat section and slightly shifted towards the convergent side of the nozzle. The flow velocity predicted from the four models is shown as a function of the axial coordinate in Fig 7. It can clearly be seen that the velocity estimated by the Bray model is very close to that predicted with the Euler model, and that both are much closer to the frozen expansion than to the shifting equilibrium one: this is in line with the early freezing point upstream of the throat section seen in Fig. 6. While the length of the converging section is similar for all models, the length of the diverging section to reach the same exit pressure (here fixed to 1 Pa) predicted by the shifting equilibrium model is much larger than the one predicted by the other models.

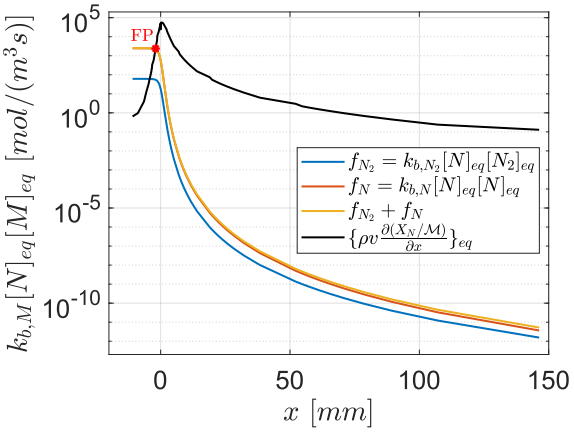

Figure 6 – Bray freezing criterion applied to the expansion of an N_2 propellant ($T_c = 8000\ K, p_c = 1\ atm$). Note the position of the freezing point (FP).

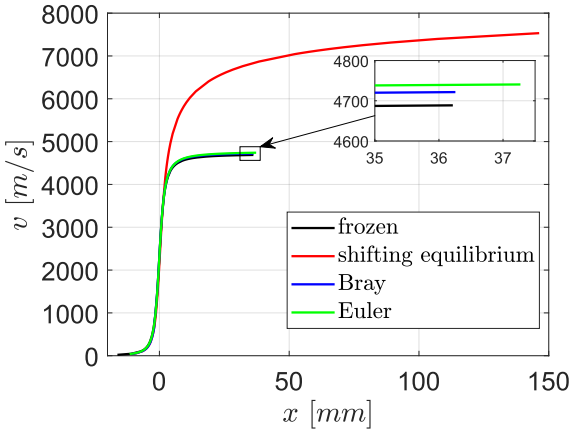

Figure 7 – Velocity as a function of the axial coordinate with different expansion models (N_2 propellant, $T_c = 8000\ K, p_c = 1\ atm, p_{out} = 1\ Pa$)

The chemical composition predicted by the Bray model is also very similar to that computed with the Euler model, as seen in Fig. 8: excluding the region close to the freezing point, where the representation is less accurate, the Bray model captures the fact that recombination processes are much slower than the flow speed and become irrelevant quite early in the expansion. This leads to an almost frozen-like expansion, with atomic nitrogen remaining the most present species all the way down to the exit conditions.

This analysis shows that the Bray model can be used, at least as a first approximation, to estimate the nozzle exit velocity and understand if the expansion is closer to the frozen or the shifting equilibrium one.

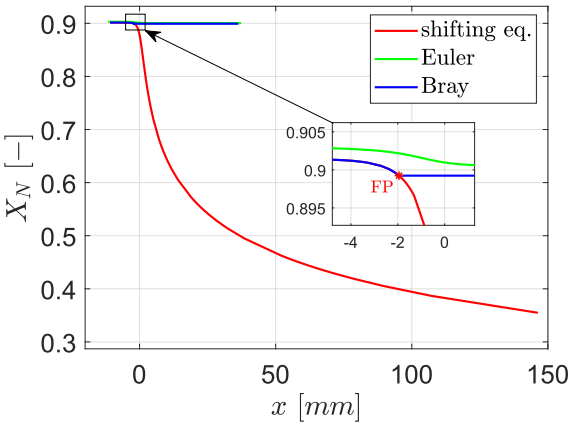

Figure 8 – Atomic nitrogen molar fraction as a function of the axial coordinate with different expansion models (N_2 propellant, $T_c = 8000\ K, p_c = 1\ atm, p_{out} = 1\ Pa$). Note the position of the freezing point FP.

4.3 Nozzle expansion for the three propellants

The exit velocity corresponding to an exit pressure of 1 Pa has been estimated using the frozen, the shifting equilibrium and the Bray expansion models for N_2, N_2O and H_2O propellants, using the procedures described in section 3. This has been repeated for a wide range of specific power values, for which the corresponding chamber temperatures are found in Fig. 5. The specific impulse has then been computed by means of equation (2) and is shown in Fig. 9-11 as a function of the specific power. Note that the lines for the Bray model are only used for visual aid, while the computed points are those displayed as the asterisks.

A wide performance gap is seen for all propellants between the frozen flow and the chemical equilibrium model, with the latter predicting higher exit velocities and corresponding specific impulse. This difference is larger for higher specific power levels (i.e., higher chamber temperatures) which correspond to higher nozzle-inlet dissociation degrees, and thus more available enthalpy to be recovered during the expansion. It is evident that for all the propellants the Bray model predicts nozzle expansions close to the frozen case, with just a marginal departure and performance increase at the high specific powers (corresponding to chamber temperatures above 8000 K), more visible in the case of H_2O. As we are considering high enthalpy flows with high velocities, happening across nozzles of very reduced dimensions (just a few centimetres), the recombination

reactions do not have enough time to happen during the expansion. This analysis suggests that when studying the nozzle expansion of METs the frozen flow assumption may be used instead of the shifting equilibrium one to provide a better approximation.

It is true on one side that this study does not keep into account the presence of the plasma in the resonant cavity, which might alter the nozzle inlet composition significantly with many more ions and excited species, and that it might be necessary to identify other chemical reactions that could shift the position of the freezing point further down the nozzle. However, as this study strongly suggests, we cannot expect to benefit much from enthalpy recovery in MET nozzles, and frozen flow losses are likely to be inevitable.

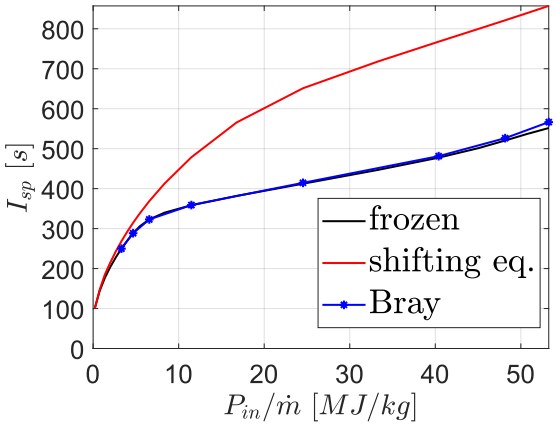

Figure 9 – Specific impulse as a function of the specific power with different expansion models (N_2 propellant, $p_c = 1\ atm, p_{out} = 1\ Pa$)

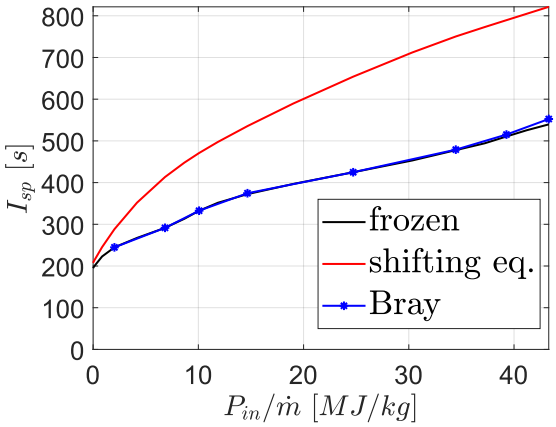

Figure 10 – Specific impulse as a function of the specific power with different expansion models (N_2O propellant, $p_c = 1\ atm, p_{out} = 1\ Pa$)

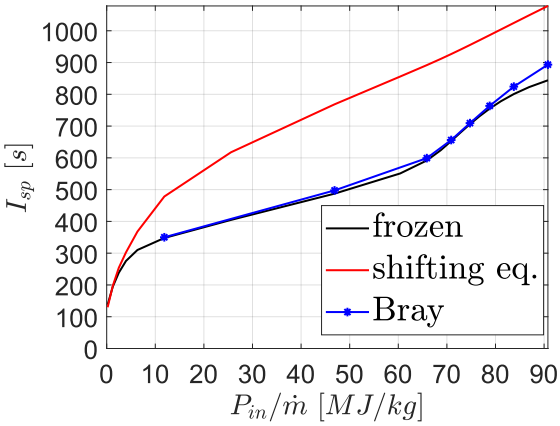

Figure 11 – Specific impulse as a function of the specific power with different expansion models (H_2O propellant, $p_c = 1\ atm, p_{out} = 1\ Pa$)

4.4 Heat transfer analysis

The heat transfer model described in section 3.3 has been applied to estimate the wall temperatures and heat flux in the nozzle during the expansion of a H_2O propellant from chamber conditions of $T_c = 6000\ K$ and $p_c = 1\ atm$, to an exit pressure $p_{out} = 1\ Pa$. The specific impulse corresponding to such conditions predicted with the Bray model is about 656 s, with a required specific power of about 71 MJ/kg. As seen in Fig. 12, the estimated Reynolds number remains low throughout the entire expansion and we can therefore assume that the flow is laminar [21], justifying the choice of the laminar correlation for the convective heat transfer coefficient in equation (22).

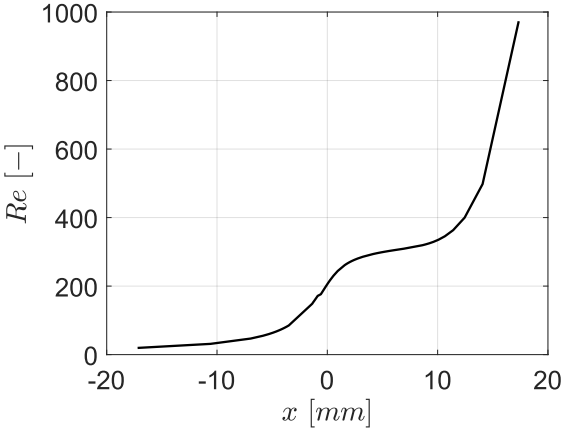

Figure 12 – Reynolds number as a function of the axial coordinate (H_2O propellant, $T_c = 6000\ K, p_c = 1\ atm, p_{out} = 1\ Pa$)

The results of this study applied to the two nozzles (t_w of 1 and 5 mm) are shown in Fig. 13 (temperature profiles) and Fig.14 (inner wall heat flux). For the nozzle with t_w of 1 mm, the inner and outer wall temperatures are almost overlapping because of the small nozzle thickness: they slowly increase from about 3000 K at the nozzle inlet to a peak of about 3300 K close to the nozzle throat, and then rapidly drop and become close to the gas temperature in the diverging section of the nozzle. A similar increasing-decreasing trend can be observed for the heat flux, which peaks at 816 W/cm^2 before becoming negligible in the divergent section. The total dissipated power is estimated to be about 792 W.

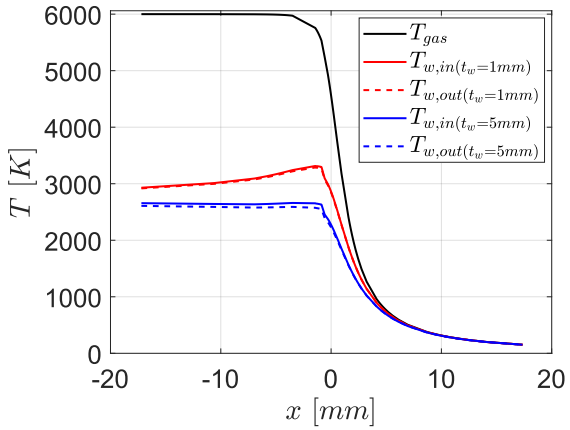

Figure 13 – Temperature profiles as a function of the axial coordinate for different nozzle thicknesses (H_2O propellant, $T_c = 6000\ K, p_c = 1\ atm, p_{out} = 1\ Pa$)

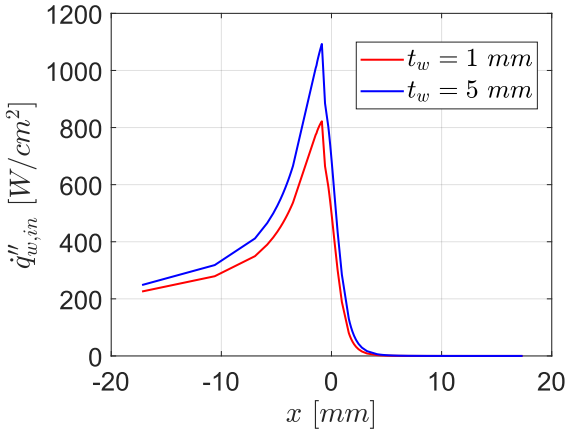

Figure 14 – Inner wall heat flux as a function of the axial coordinate for different nozzle thicknesses (H_2O propellant, $T_c = 6000\ K, p_c = 1\ atm, p_{out} = 1\ Pa$)

The nozzle throat is the most critical section in terms of temperatures and heat flux because of the small diameter. In fact, the predicted wall temperatures at the throat section are not very far from the melting point of tungsten (3687 K [24]), meaning that under these steady state operating conditions the nozzle could undergo plastic deformation processes leading it to thermo-mechanical failure. The situation in terms of temperatures can be improved using the nozzle with t_w of 5 mm, for which the inner wall temperatures remain roughly constant at 2650 K in the entire converging section and then again drop and become close to the gas temperature in the diverging section. The drawback of the nozzle with thicker walls is a larger heat flux (peak of 1087 W/cm^2) due to the larger gas-wall temperature drop, which results in a higher dissipated power (928 W).

An important observation comes from the dissipated power itself. The mass flow rate for this expansion is $\dot{m} \approx 19.3\ mg/s$, which combined with the 71 MJ/kg of specific power yields a required input power of about 1370 W. This means that roughly 58-68% of the microwave power added to the propellant in the resonant cavity would be lost immediately through heat dissipation in the nozzle walls (for nozzle thicknesses of 1-5 mm, respectively). Even though a thinner nozzle can reduce the fraction of lost power, this cannot be reduced indefinitely because, as seen from Fig. 13, wall temperatures will increase, and they are already critical with a nozzle thickness of 1 mm. These numbers suggest that it might be worth investigating the feasibility and convenience of regenerative nozzle cooling methods to recycle the waste power and pre-heat the propellant before injecting it into the resonant cavity. Furthermore, and most importantly, since the power lost per unit mass flow rate is of the same order of magnitude of the flow specific enthalpy, the effects of such a large power loss to the nozzle walls cannot be neglected when modeling the gas dynamic expansion, and they may result in a significant performance drop. Therefore, future accurate descriptions of nozzle expansions for METs working at high chamber temperatures should include modeling of heat losses to the nozzle walls.

Although the nozzle size and geometry for a MET don't necessarily need to be the same used in this study, the order of magnitude of the dimensions is likely to remain the same, with throat diameters not larger than a few millimeters. Thus, at the conditions required for I_{sp} of about 650 s with H_2O, the nozzle wall temperatures and heat fluxes are going to be significant and similar to those shown here. The situation is potentially even worse with the other propellants, because the required chamber

temperatures to obtain the same specific impulse with N_2 and N_2O would need to be larger than 10000 K (see Fig. 5, 9 and 10).

5. Conclusions

The nozzle expansion of different propellants (N_2, N_2O and H_2O) for a MET has been studied using a Bray expansion model to estimate the specific impulse. The nozzle inlet conditions for all models and propellants have been obtained assuming chemical equilibrium in the resonant cavity.

The Bray model has first been validated using the Euler model with chemical reactions for the case of a N_2 expansion, with a good agreement on both the velocity field and the composition, indicating that it can be used as a reasonable approximation of the exact model. Then, it has been compared to the frozen and the shifting equilibrium solutions for different chamber temperatures. For all propellants and most chamber temperatures, the Bray model predicts nozzle exit velocities and corresponding specific impulses very close to the one given by the frozen flow model, with just a small relative increase at the high temperatures, implying that frozen flow losses are likely to be present and very marginal enthalpy recovery is possible in the nozzle.

Finally, a heat transfer analysis has been carried out on a representative case study of the H_2O propellant expansion through a passively cooled nozzle. Considerable temperatures and heat fluxes have been estimated at the internal nozzle walls, suggesting the possible need of active and regenerative cooling methods to obtain specific impulses larger than 650 s. The estimated power per unit mass flow rate dissipated through the nozzle walls amounts to about two thirds of the flow's specific enthalpy, indicating that a more accurate description of the expansion requires modeling of the wall heat losses. The development of quasi-1D models which include this term is foreseen in the near future, in order to evaluate its impact on the flow properties and, ultimately, the propulsive performance.

Appendix A (ODE system for Euler model)

Using equations (18), (19) and (20), combined with the Arrhenius form for the reaction coefficients (16), the system of equations (17) can be rewritten more conveniently as a system of four ordinary differential equations, in the variables Y, v, ρ and T:

$$\begin{cases} \dfrac{dY}{dx} = \dfrac{\rho T^{\eta_k}}{v\mathcal{M}_N}\left[C_{b,N_2}\dfrac{1-Y}{2} + C_{b,N}Y\right]\left[(1-Y)\,exp\left(-\dfrac{\theta_k}{T}\right) - Y^2\dfrac{\rho}{\rho_D}\right] \\ \dfrac{dv}{dx} = \dfrac{\left[(1+Y)\left(\dfrac{dY}{dx}\left(\dfrac{\partial e}{\partial Y}\right)_T\left(\dfrac{\partial e}{\partial T}\right)_Y^{-1} + (1+Y)R_{N_2}T\left(\dfrac{\partial e}{\partial T}\right)_Y^{-1}\dfrac{d(lnA)}{dx} + \dfrac{T}{A}\dfrac{dA}{dx}\right) - \dfrac{dY}{dx}\right]}{\left[\dfrac{v}{R_{N_2}} - \dfrac{(1+Y)^2R_{N_2}T}{v}\left(\dfrac{\partial e}{\partial T}\right)_Y^{-1} - (1+Y)\dfrac{T}{v}\right]} \\ \dfrac{d\rho}{dx} = -\dfrac{\rho}{v}\dfrac{dv}{dx} - \dfrac{\rho}{A}\dfrac{dA}{dx} \\ \dfrac{dT}{dx} = -\left(\dfrac{\partial e}{\partial T}\right)_Y^{-1}\left[\left(\dfrac{\partial e}{\partial Y}\right)_T\dfrac{dY}{dx} + \dfrac{(1+Y)R_{N_2}T}{v}\dfrac{dv}{dx} + (1+Y)TR_{N_2}\dfrac{d(lnA)}{dx}\right] \end{cases}$$

where the differential terms in the brackets $(\dots)_T$ and $(\dots)_Y$ are evaluated at constant temperature and mass fraction, respectively, and the expression for the area and its derivatives can be obtained starting from equation (4). This system of equations is fully coupled, because the derivative of each state variable depends on one or more of the other variables, and the four equations must thereby be solved simultaneously.

References

[1] A. Sarritzu, F. Lauck, L. Werling, A. Pasini, Assessment of propulsion system architectures for green propellants-based orbital stages, 73rd International Astronautical Congress (IAC), Paris, France, 2022, 18-22 September.

[2] D. O'Reilly, G. Herdrich, D. F. Kavanagh. Electric propulsion methods for small satellites: A review. Aerospace, 8(1) (2021) 22. https://doi.org/10.3390/aerospace8010022

[3] S. Mazouffre, Electric propulsion for satellites and spacecraft: established technologies and novel approaches, Plasma Sources Science and Technology 25(3) (2016) 033002. https://doi.org/10.1088/0963-0252/25/3/033002

[4] K.D. Diamant, B.L. Zeigler, R.B. Cohen, Microwave electrothermal thruster performance, Journal of Propulsion and Power 23(1) (2007) 27 – 34. https://doi.org/10.2514/1.19571

[5] Micci, M.M., Bilen, S.G., Clemens, D.E.: History and current status of the microwave electrothermal thruster. EUCASS Proceedings Series 1(13) (2009) 425 – 438. https://doi.org/10.1051/eucass/200901425

[6] Brandenburg, J.E., Kline, J., Sullivan, D.: The microwave electro-thermal (met) thruster using water vapor propellant. IEEE Transactions on Plasma Science 33(2), 776 – 782 (2005). https://doi.org/10.1109/TPS.2005.845252

[7] A. E. Nosseir, A. Cervone, A. Pasini, Review of state-of-the-art green monopropellants: For propulsion systems analysts and designers, Aerospace, 8(1) (2021) 20. https://doi.org/10.3390/aerospace8010020

[8] J. L. Rovey, C.T. Lyne , A. J. Mundahl, N. Rasmont, M. S. Glascock, M. J. Wainwright, S. P. Berg, Review of multimode space propulsion. Progress in Aerospace Sciences, 118 (2020) 100627. https://doi.org/10.1016/j.paerosci.2020.100627

[9] J. Lee, L. L. Raja, A numerical investigation of the micronozzle geometry effect on the performance of microwave electrothermal thrusters, AIAA 2023-3480, AIAA AVIATION Forum, San Diego, California, USA, 2023, 12-16 June. https://doi.org/10.2514/6.2023-3480

[10] J. Lee, L. L. Raja, Computational study of a helium-propellant microwave electrothermal thruster, Journal of Applied Physics 135 (2024). https://doi.org/10.1063/5.0190223

[11] G.P. Sutton, O. Biblarz, Rocket Propulsion Elements, ninth ed., John Wiley and Sons, Inc., New Jersey 2017.

[12] D.E. Clemens. Performance evaluation of the Microwave Electrothermal Thruster using Nitrogen, simulated Hydrazine and Ammonia. PhD thesis, The Pennsylvania State University, 2008.

[13] Ruscic, B., Bross, D.H.: Active thermochemical tables (atct) thermochemical values ver. 1.122r (2021). https://doi.org/10.17038/CSE/1822363

[14] K. N. C. Bray, Chemical reactions in supersonic nozzle flows, Symposium (International) on Combustion, 9 (1) (1963) 770-784. https://doi.org/10.1016/S0082-0784(63)80085-5

[15] L. T. De Luca, Problemi energetici in propulsione aerospaziale: appunti per studenti, first ed., Companion CD, Milano 1997.

[16] S. Gordon, B. J. McBride, Computer Program for Calculation of Complex Chemical Equilibrium Compositions and Applications. NASA Lewis Research Center, Cleveland, OH (1994).

[17] F. Dias, J. Páscoa, C. Xisto, Numerical Analysis of a Multi-Species MHD Model for Plasma Layer Control of Re-Entry Vehicles, Proceedings of the ASME 2018 International Mechanical Engineering Congress and Exposition. Volume 1: Advances in Aerospace Technology, Pittsburgh, Pennsylvania, USA, 2015, 9–15 November. https://doi.org/10.1115/IMECE2018-87467

[18] V. J. Sarli, W. G. Burwell, R. Hofland JR., T. F. Zupnik, Evaluation of the Bray sudden-freezing criterion for predicting nonequilibrium performance in multireaction rocket nozzle expansions, AIAA Propulsion Joint Specialist Conference, Colorado Springs, Colorado, USA 1965, 14-18 June. https://doi.org/10.2514/6.1965-554

[19] A. H. Shapiro, The dynamics and thermodynamics of compressible fluid flow, first ed., Wiley, New York 1953.

[20] M. J. Lighthill, Dynamics of a dissociating gas Part I Equilibrium flow, Journal of Fluid Mechanics, 2(1) (1957) 1-32. https://doi.org/10.1017/S0022112057000713

[21] B. Jacimovic, S. Genic, D. Lelea, Calculation of the Heat Transfer Coefficient for Laminar Flow in Pipes in Practical Engineering Applications, Heat Transfer Engineering, 39(20) (2017) 1790–1796. https://doi.org/10.1080/01457632.2017.1388949

[22] R. A. Svehla, Transport Coefficients for the NASA Lewis Chemical Equilibrium Program, NASA Technical Memorandum 4647, Cleveland, OH (1995).

[23] B. J. McBride, M. J. Zehe, S. Gordon, NASA Glenn Coefficients for Calculating Thermodynamic Properties of Individual Species, NASA/TP—2002-211556, Cleveland, OH (2002).

[24] J. W. Arblaster, Thermodynamic Properties of Tungsten. Journal of Phase Equilibria and Diffusion, 39 (2018) 891–907. https://doi.org/10.1007/s11669-018-0689-1